[CANCER RESEARCH 61, 6524–6531, September 1, 2001]

Mapping Extracellular pH in Rat Brain Gliomas *in Vivo* by ^{1}H Magnetic Resonance Spectroscopic Imaging: Comparison with Maps of Metabolites[1]

María-L. García-Martín, Gwénaël Hérigault,[2] Chantal Rémy, Régine Farion, Paloma Ballesteros, Jonathan A. Coles, Sebastián Cerdán, and Anne Ziegler[3]

Instituto de Investigaciones Biomédicas, Consejo Superior de Investigaciones Cientificas, 28029 Madrid, Spain [M-L. G-M., S.C.]; Unité mixte Institut National de la Santé et de la Recherche Médicale/Université Joseph Fourier: U438 "RMN Bioclinique," Laboratoire de Recherche Correspondant du Commissariat à l'Energie Atomique, Centre Hospitalier Universitaire BP 217, 38043 Grenoble, France [G. H., C. R., R. F., J. A. C., A. Z.]; and Departemento de Química Orgánica y Biología, Facultad de Ciencias, Universidad Nacional de Educación a Distancìa, 28040 Madrid, Spain [P. B.]

ABSTRACT

The value of extracellular pH (pH_e) in tumors is an important factor in prognosis and choice of therapy. We demonstrate here that pH_e can be mapped *in vivo* in a rat brain glioma by ^{1}H magnetic resonance spectroscopic imaging (SI) of the pH buffer (±)2-imidazole-1-yl-3-ethoxycarbonylpropionic acid (IEPA). ^{1}H SI also allowed us to map metabolites, and, to better understand the determinants of pH_e, we compared maps of pH_e, metabolites, and the distribution of the contrast agent gadolinium1,4,7,10-tetraazacyclododecane-N,N′,N″,N‴-tetraaceticacid (Gd-DOTA). C6 cells injected in caudate nuclei of four Wistar rats gave rise to gliomas of ~10 mm in diameter. Three mmols of IEPA were injected in the right jugular vein from $t = 0$ to $t = 60$ min. From $t = 50$ min to $t = 90$ min, spin-echo ^{1}H SI was performed with an echo time of 40 ms in a 2.5-mm slice including the glioma (nominal voxel size, 2.2 μl). IEPA resonances were detected only within the glioma and were intense enough for pH_e to be calculated from the chemical shift of the H2 resonance in almost all voxels of the glioma. ^{1}H spectroscopic images with an echo time of 136 ms were then acquired to map metabolites: lactate, choline-containing compounds (tCho), phosphocreatine/creatine, and N-acetylaspartate. Finally, T_1-weighted imaging after injection of a bolus of Gd-DOTA gave a map indicative of extravasation. On average, the gradient of pH_e (measured where sufficient IEPA was present) from the center to the periphery was not statistically significant. Mean pH_e was calculated for each of the four gliomas, and the average was 7.084 ± 0.017 (± SE; $n = 4$ rats), which is acid with respect to pH_e of normal tissue. After normalization of spectra to their water peak, voxel-by-voxel comparisons of peak areas showed that N-acetylaspartate, a marker of neurons, correlated negatively with IEPA ($P < 0.0001$) and lactate ($P < 0.05$), as expected of a glioma surrounded by normal tissue. tCho (which may indicate proliferation) correlated positively with pH_e ($P < 0.0001$). Lactate correlated positively with tCho ($P < 0.0001$), phosphocreatine/creatine ($P < 0.001$), and Gd-DOTA ($P < 0.0001$). Although lactate is exported from cells in association with protons, within the gliomas, no evidence was observed that pH_e was significantly lower where lactate concentration was higher. These results suggest that lactate is produced mainly in viable, well-perfused, tumoral tissue from which proton equivalents are rapidly cleared.

INTRODUCTION

pH_i[4] in tumor cells is normal or slightly alkaline; in contrast, pH_e is usually acid compared with normal tissue and, unlike pH_i, appears to vary with the type of tumor (1–3) so that measurement of pH_e is potentially more informative than measurement of pH_i. Knowledge of pH_e is important not only for diagnosis but also for choosing chemotherapeutic agents, because most are weak bases or weak acids, and their accumulation within cells and, hence, their efficacy depends on the transmembrane pH gradient (1, 4–7). In addition, the effectiveness of thermoradiotherapy has been reported to correlate with the extracellular acidity (8). Therefore, noninvasive measurement of tumor pH_e might be useful for diagnosis, choice of therapy, and prognosis.

Tumor pH_e has been measured mainly by invasive techniques that measure it at a single point, namely microelectrodes (9, 10) and miniature optical probes (11). The value of these measurements depends on how uniform pH_e is throughout the tumor. Mean pH_e within tumors has also been measured noninvasively by NMR using extracellular probe molecules containing ^{31}P or ^{19}F (6, 12–14). Spatial variations in pH_e have been measured over distances in the order of 100 μm in the tissue between blood vessels in the exposed superficial layers of a s.c. tumor by optical techniques (15). In the present work, we have made maps of pH_e on a larger scale throughout sections of C6 gliomas in rat brain. The tool we used is a new probe molecule, which has pH-dependent ^{1}H resonances detectable by ^{1}H NMR spectroscopy. This molecule is IEPA. It has been shown that IEPA does not enter erythrocytes (compound 9 in Ref. 16), and it appears to remain extracellular in a tumor model in a mouse mammary fat pad where the ^{1}H signal was sufficient for SI (17). Preliminary results had shown that systemically delivered IEPA infiltrates the extracellular space of C6 gliomas in brain and allows mapping of pH_e (18).

In addition to providing a signal:noise ratio sufficient to allow imaging of pH_e rather than just measurement of the average value in a volume including the tumor, detection by ^{1}H magnetic resonance spectroscopy has an additional advantage: using the same radiofrequency coil, the distributions of various endogenous compounds with ^{1}H resonances can be readily imaged in the same experiments. These include compounds of which the concentrations might be causally related to the value of pH_e, notably lactate. Hence, in this paper, we not only report the use of IEPA to image the distribution of pH_e within C6 gliomas, but we have compared this distribution with the distribution of lactate and also of tCho, NAA, and tCr. The results lead us to consider the reasons why pH_e in C6 gliomas should be acid. Both normal brain tissue (19) and tumor cells in particular (20, 21) produce lactate even under aerobic conditions. Lactate is exported from cells in association with H^+ (22) and in this way is expected to contribute to the extracellular acidity. However, Yamagata *et al.* (23) and Newell *et al.* (24) have found that even tumor cells lacking lactate dehydrogenase, which produced very little lactate *in vitro*, nevertheless created an acid extracellular environment when grown as tumors. By using IEPA, we have been able to see whether the distribution of pH_e correlated with that of lactate *in vivo*.

Received 2/27/01; accepted 6/29/01.

The costs of publication of this article were defrayed in part by the payment of page charges. This article must therefore be hereby marked *advertisement* in accordance with 18 U.S.C. Section 1734 solely to indicate this fact.

[1] Supported in part by an Institut National de la Santé et de la Recherche Médicale-Consejo Superior de Investigaciones Cientificas Collaborative Grants and grants 08.1/0023/1997 and 08.1/0046/1998 (to S. C.); a Strategic Group Grant (to P. B.) from the community of Madrid; and grants from La Ligue contre le Cancer, l'Association pour la Recherche sur le Cancer, and the Région Rhone-Alpes (to C. R.).

[2] Present address: Department of Radiology, Box 8131, Washington University School of Medicine, 660 South Euclid, St. Louis, MO 63110.

[3] To whom correspondence should be addressed, at INSERM U438, CHU Pavillon B, BP 217, 38043 Grenoble Cedex 9, France.

[4] The abbreviations used are: pH_i, intracellular pH; NMR, nuclear magnetic resonance; pH_e, extracellular pH; NAA, N-acetylaspartate; SI, spectroscopic imaging; tCho, total choline-containing compounds; tCr, creatine and creatine phosphate; CHESS, chemical-shift selective excitation; OVS, outer volume saturation; TE, echo time; TR, repetition time; T_2: transverse relaxation time; pH_a, arterial pH; Gd-DOTA, gadolinium1,4,7,10-tetraazacyclododecane-N,N′,N″,N‴-tetraaceticacid; IEPA, (±)2-imidazole-1-yl-3-ethoxycarbonylpropionic acid; ppm, parts per million; WSI, water spectroscopic imaging.

Downloaded from http://aacrjournals.org/cancerres/article-pdf/61/17/6524/2486551/ch1701006524.pdf by guest on 13 August 2024

MATERIALS AND METHODS

IEPA was synthesized as described previously, with the preparation more than 99.9% pure as determined by gas chromatography and mass spectrometry (16). C6 cells were a gift from P. Canioni, Bordeaux University, and DMEM culture medium was purchased from Life Technologies, Inc. Isoflurane was obtained from Abbott Laboratories (Abbott Park, IL). Other reagents were from Sigma Chemical Co. (St. Louis, MO).

Calibration of the pH Dependence of the Chemical Shift of the IEPA H2 Resonance. Fifteen vials containing solutions of 20 mM IEPA and 100 mM of the HEPES buffer in rat plasma were titered at 37°C with HCl or NaOH to pHs in the range 4.5–8.5. The chemical shift of the IEPA H2 hydrogen and its T_2 were measured at 37°C using an 8.4 Tesla magnet (Oxford Instruments, United Kingdom) interfaced with an AM-360 NMR spectrometer (Bruker, Karlsruhe, Germany). We used a single pulse sequence with a 1 s presaturating pulse on the water resonance to decrease the water resonance intensity. The excitation pulse duration was 7 μs, data size 16384 points, and acquisition time 0.95 s. pH titrations of the H2 chemical shift were fitted using Sigmaplot v 4.0 (SPSS Inc., Chicago, IL) with the Henderson-Hasselbalch equation:

$$pH = pK_a + \log\frac{(\delta_1 - \delta)}{(\delta - \delta_2)} \quad (1)$$

where δ is the chemical shift and $\delta_1 > \delta_2$ are the asymptotic values.

The T_2 of IEPA H2 and H5 peaks were also determined in the same samples used for the pH titration. The Hahn spin-echo sequence was modified to include a 1-s selective presaturating pulse, a jump and return excitation pulse (interpulse delay, 210 μs), and a binomial refocusing pulse (interpulse delay, 420 μs; Ref. 25). Ten different values of TE in the range 2–400 ms were used to obtain T_2 at different pHs. T_2(H2) showed a minimum of 43 ms at pH 6.5 increasing to 81 ms at pH 4.5 and to 100 ms at pH 8.5. Although this variation in T_2 does not affect the calculation of pH from the chemical shift, it would affect the apparent distribution of IEPA. Therefore, the distribution of IEPA was calculated from the H5 peak of which the T_2 did not vary significantly over the pH range 5.5–7.5 ($T_2 = 57 \pm 4$ ms).

Animal Preparation. All of the procedures involving animals conformed to the guidelines of the French Government (decree 87–848, October 19, 1987, licenses 006683 and A38071). To prepare the glioma model, Wistar rats (200–230 g) were anesthetized with chloralhydrate (400 mg/kg), and $\sim 10^5$ C6 glioma cells (26) in DMEM were injected stereotaxically in the right caudate nucleus (as in Refs. 27, 28 but without the use of agar). Gliomas developed, which, after 3 weeks, occupied 30–50% of the right hemisphere of the brain. All of the rats were females except for one male included in the results shown in Fig. 4.

To prepare the rats for NMR experiments, anesthesia was induced with 4% isoflurane in air delivered to a mask and then maintained with a mixture of 0.7–1.2% (v/v) isoflurane in air enriched with oxygen to 30% (v/v). The fractional inspired oxygen was continuously monitored with a polarimetric cell (Pro-Custom Elettronica, Milan, Italy). A 0.7-mm indwelling catheter was inserted into the right jugular vein. For IEPA mapping, 6-ml 0.5 M of a solution of IEPA in deionized water, pH adjusted to 7.2 with NaOH, was infused in the right jugular vein over 60 min to give a total quantity of $\leq$15 mmol/kg body weight. Another 0.7-mm indwelling catheter was inserted into the left femoral artery. Blood gases (P_aO_2 and P_aCO_2), arterial oxygen saturation of hemoglobin (S_aO_2), pH_a, and hemoglobin content were measured in arterial blood samples of $<$0.1 ml (ABL 510; Radiometer, Copenhagen, Denmark) before the beginning of the IEPA infusion and subsequently at 40 min intervals up to 2 h (Fig. 1). Rectal temperature was maintained at 36.5–37.5°C by a heating pad placed on the abdomen. Measurements of blood gases and pH_a were corrected for rectal temperature. pH_a was in the range 7.28–7.45, and during the NMR imaging, arterial carbon dioxide pressure was in the range 32–40 mm of Hg. At the end of the cycle of measurements, the animal was killed by an overdose of chloralhydrate.

***In Vivo* NMR Measurements.** Experiments were carried out with a SMIS console (Surrey Medical Imaging Systems Ltd., Guildford, United Kingdom) equipped with a 20-cm horizontal bore, 7 Tesla magnet (Magnex Scientific Ltd., Abington, United Kingdom), and actively shielded gradients (Magnex). Standard NMR images were processed with the standard SMIS image-processing package. Raw NMR SI data were transferred to a Unix workstation (Sun Microsystems Inc., Palo Alto, CA) for off-line analysis. The processing software was developed in the Interactive Data Language programming environment (Research Systems International, Boulder, CO).

The rat was prone, its head secured by ear bars, and a 25-mm diameter surface coil located directly above the brain was used for radiofrequency transmission and reception. After radiofrequency coil matching and tuning, the magnetic field homogeneity was coarsely adjusted to obtain a line width for water $<$40 Hz in a 5-mm horizontal slice of the brain. Additional fine adjustments were carried out in the volume of interest for each separate NMR measurement. An idealized scheme of the experiment is shown in Fig. 1.

Spin-Echo NMR Imaging. To assess glioma development in each rat and to select a slice including the tumor for subsequent single voxel or SI experiments, scout spin-echo images were obtained (slice thickness, 1 mm; TR, 3 s; TE, 80 ms; 128 $\times$ 128 pixels, 5 horizontal slices and 7 coronal slices).

Single Voxel Spectroscopy. To follow changes in IEPA concentration and pH_e within the glioma, during the infusion of IEPA and the subsequent 2 h from a volume in the center of the glioma, experiments were made on three rats using point resolved spectroscopy (Ref. 29; TR, 3 s; TE, 40 ms; voxel size, 5 $\times$ 5 $\times$ 5 mm, 64 scans) taken at 5-min intervals. At the end of the NMR measurements, the brains were excised and the tumor dissected and frozen. The concentration of IEPA in an aqueous extract of each tumor was measured by high-resolution ^{1}H NMR spectroscopy.

^{1}H SI. The pulse sequence is shown in Fig. 2. ^{1}H spectroscopic images were acquired on four rats using a spin-echo sequence with OVS (four slices), and CHESS excitation (30) for water saturation (3-lobe-sinc pulse, 8 ms duration, followed by crusher gradients of 2 ms, 20 mT/m). For IEPA mapping (TE, 40 ms), a binomial pulse (31, 32) with a frequency response centered on 8 ppm was used for excitation, and the refocusing pulse was selective for a 2.5-mm horizontal slice (5-lobe-sinc pulses, 6 kHz). For mapping other metabolites, both excitation and refocusing pulses were slice selective (TE, 136 ms). WSI were acquired at each TE for phase and frequency shift reference. The field of view was 30 $\times$ 30 mm^2. Phase-encoding steps (32 $\times$ 32) were used with acquisition weighting (Hanning window; Ref. 33); TR was 3 s, so the total acquisition time was about 40 min. For WSI, TR was 1 s, and the total acquisition time was 8 min. Bandwidth was 10 kHz with 1024-point acquisition in the time domain. Data were filtered in the time domain using a Gaussian function resulting in a 10-Hz line broadening. Zero filling was performed in both spatial dimensions to 64 points and in the spectral dimension to 2048 points before three-dimensional Fast Fourier Transformation. After correction for frequency shifts attributable to imperfect field homogeneity and pre- and postperfusion data subtraction, the chemical shift of the IEPA H2 resonance of each voxel spectrum, of which the signal:noise ratio was $>$5, was obtained by

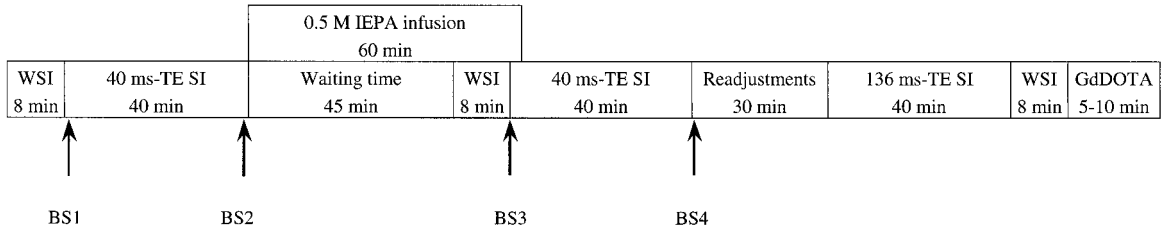

Fig. 1. Scheme showing the order in which the different kinds of NMR images were acquired after the rat was placed in the magnet. First, a WSI was acquired over 8 min, then a 40-ms TE SI was acquired to obtain baseline spectra for subsequent subtraction from spectra including IEPA signals, then IEPA was infused, and so forth. Metabolic SI had 136-ms TE; T1-weighted images (30 s each) were acquired after GdDOTA injection.

Downloaded from http://aacrjournals.org/cancerres/article-pdf/61/17/6524/2486551/ch1701006524.pdf by guest on 13 August 2024

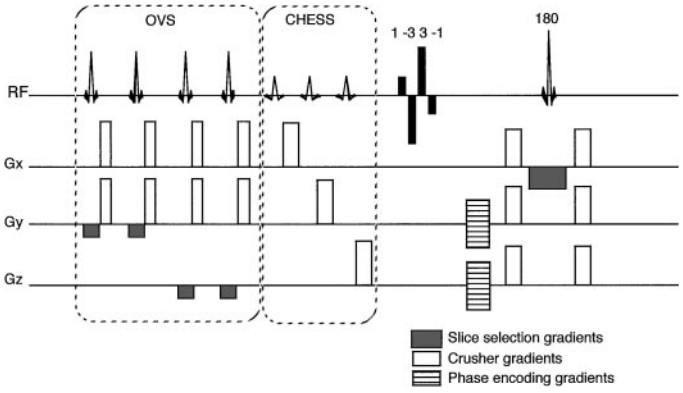

Fig. 2. The SI pulse sequence. Four slices were positioned around the volume of interest for saturation (OVS module), then three CHESS pulses were used to suppress the water signal. SI sequence is a standard spin-echo sequence, with phase-encoding gradients in the directions perpendicular to the slice selection. The crusher gradients lasted 2 ms (19 mT/m in the slice direction and 12 mT/m in the phase-encoding directions.

standard nonlinear curve-fitting using the complex Lorentzian line shape function. The chemical shift was calculated on the assumption that the water peak was at 4.70 ppm; tests showed that with this assumption the tCr peak consistently had a chemical shift of 3.03 ppm in agreement with previous measurements (34). pH was then obtained from the titration equation (Eq. 1). In a small minority of voxels, two peaks within the range of the H2 resonance were observed; in these cases, the larger peak was fitted. In the spectra obtained with the longer TE, the areas of the peaks assigned to lactate (1.31 ppm), NAA (2.03 ppm), tCho (3.23 ppm), tCr (3.03 ppm), and lipids (1.26 ppm) were calculated. Peak areas in each voxel were then normalized with respect to the water peak to correct for instrumental variations between experiments.

T_1-weighted Imaging. To image the regions of perfusion and extravasation in the same 2.5-mm slice as for SI, Gd-DOTA (0.1 mmol/kg body weight; Dotarem, Guerbet, Aulnay-sous-Bois, France) was injected in the right jugular vein, and a series of spin-echo images were acquired at 40-s intervals with TR, 500 ms; TE, 30 ms; acquisition time, 32 s.

Histology. After the imaging experiment, the brain was excised and fixed in 10% formol for 48 h and embedded in paraffin. Horizontal sections of the glioma 3-μm thick were stained with H&E.

Errors of Measurement. These have been considered in detail by van Sluis *et al.* (17). We estimate that the uncertainty in the constants in the equation fitted to the *in vitro* pH calibration points (Eq. 1; Fig. 3*e*) leads to an uncertainty of ~0.035 pH units in our estimates of the absolute scale of values of pH_e for all of the *in vivo* measurements. In addition, the uncertainty in the determination of the chemical shift of the H2 peak in the spectrum for each voxel is estimated to lead to a random error of 0.01 pH units for each voxel. Hence, our estimates of absolute values of pH_e, averaged over many voxels, may be in error by 0.035 pH units. On the other hand, the maximum error in the difference of pH_e between one voxel and another should be $2 \times 0.01 = 0.02$ pH units.

Data Analysis. The spatial distributions of pairs of quantities (*e.g.*, lactate signal and pH_e) were compared by calculating the Pearson correlation coefficient defined by

$$r_{xy} = \frac{S_{xy}^2}{\sqrt{S_x^2 S_y^2}}$$

where $S_x^2 = \Sigma(X_i - <X>)^2$ and $S_{xy}^2 = \Sigma(X_i - <X>)(Y_i - <Y>)$, and X_i, Y_i are the values of the two quantities in voxel i.

RESULTS

Imaging pH_e in a Glioma. Fig. 3*c* is a T_1-weighted image of a horizontal section of a glioma-bearing rat brain acquired over 32 s starting ~80 s after injection of a bolus of Gd-DOTA in the right jugular vein. The marked hyperintensity in the periphery of the glioma corresponded to well-perfused regions with leaky blood vessels (35). Comparison with the histology confirmed that large central parts of the glioma from which the signal was weak corresponded to necrotic regions. Before the injection of Gd-DOTA, IEPA had been infused during 60 min into the right jugular vein and ^{1}H spectra with a 40-ms TE obtained from each voxel of a slice (see Fig. 1). After infusion of IEPA, the spectra from the contralateral hemisphere were unchanged (Fig. 3*a*) but new peaks appeared in the glioma. A double peak near 7.2 ppm corresponded to the H4 and H5 resonances of IEPA, which are relatively insensitive to pH, and a peak near 8 ppm corresponded to the pH-sensitive H2 resonance (arrow in Fig. 3*b*; Refs. 16, 17). Analysis of the spectra showed that within the brain, signals from IEPA reached our criterion amplitude (5 times the noise) only within the glioma. The area under the H5 peak was measured for each voxel and a map made (Fig. 3*d*). To relate the chemical shift of the H2 peak to pH, we made an *in vitro* calibration curve for IEPA in plasma at 37°C, which showed that the chemical shift of the IEPA H2 proton varied from 7.72 ppm (δ_2) to 8.85 ppm (δ_1) with a pK_a of 6.566 ± 0.035 (Fig. 3*e*). By use of this curve, pH_e was calculated for each voxel and a map constructed (Fig. 3*f*). This could only be done where IEPA was present, so there are no valid measurements for normal tissue or for the center of the necrotic core. The maps showed variations in pH_e within the glioma over a range of ~0.4 pH units (Figs. 3*f* and 6*h*), but no marked and significant general trend was observed (*e.g.*, from the center to the periphery). The mean value of pH_e measured in the regions infiltrated by IEPA in each glioma was calculated; the mean value for the four gliomas was 7.084 ± 0.017 (±SE). This is well below the pH of the arterial blood, which was monitored in all of the experiments and found to remain within the range 7.33–7.41 during the IEPA imaging. In almost all of the voxels, only one H2 peak was detected. In a few voxels there were two peaks, but both peaks always corresponded to pHs more acidic than that of the circulating blood (~7.4). We failed to detect any association of the presence of two peaks with any other feature of the gliomas. In agreement with the majority of previous results in other tumors and tumor models made using other methods of measurement, pH_e in the C6 glioma was lower than the values most frequently reported for normal brain tissue (~7.3; Ref. 6).

Fig. 4 presents results that relate to the possibility that the presence of IEPA in the extracellular clefts modified pH_e. pH_e was measured in a single large voxel covering about one-half the volume of the glioma. During the infusion of IEPA, as the quantity in the glioma increased 3-fold, pH_e changed little and may have fallen slightly. After the end of the perfusion (from 60 to 130 min), there was a small but significant increase in pH_e: a linear regression gave $pH_e = 7.036 + 0.00127 \times (t/\text{min})$, $r^2 = 0.87$. Thus, in comparing pH_e in the presence of high and low concentrations of IEPA, these results show that a high mean concentration of IEPA was associated with a slightly more acidic pH_e.

Maps of Metabolites. Fig. 5 shows typical ^{1}H spectra obtained with a TE of 136 ms from normal tissue (*a*) and from the periphery (*b*) and center (*c*) of a glioma. Because of the J-coupling modulation, the lactate peak is negative and, for this reason, its partial overlap with the lipid peak causes an apparent shift of both chemical shifts and may distort the amplitudes when both peaks are present. Because obtaining IEPA images was the main methodological innovation of the work, the IEPA images were obtained before the metabolic images, the latter being acquired 120–160 min after the beginning of the IEPA infusion (Fig. 1). By this time, little IEPA (~20% of the maximum) still remained in the glioma (Fig. 4). If residual IEPA contaminated the metabolic spectra, the peak most likely to do so was the triple resonance from the IEPA methyl group. In spectra obtained from extracts of gliomas (from other rats, not shown) this IEPA peak was at 1.17 ppm. We conclude that it is unlikely that the IEPA methyl peak

Downloaded from http://aacrjournals.org/cancerres/article-pdf/61/17/6524/2486551/ch1701006524.pdf by guest on 13 August 2024

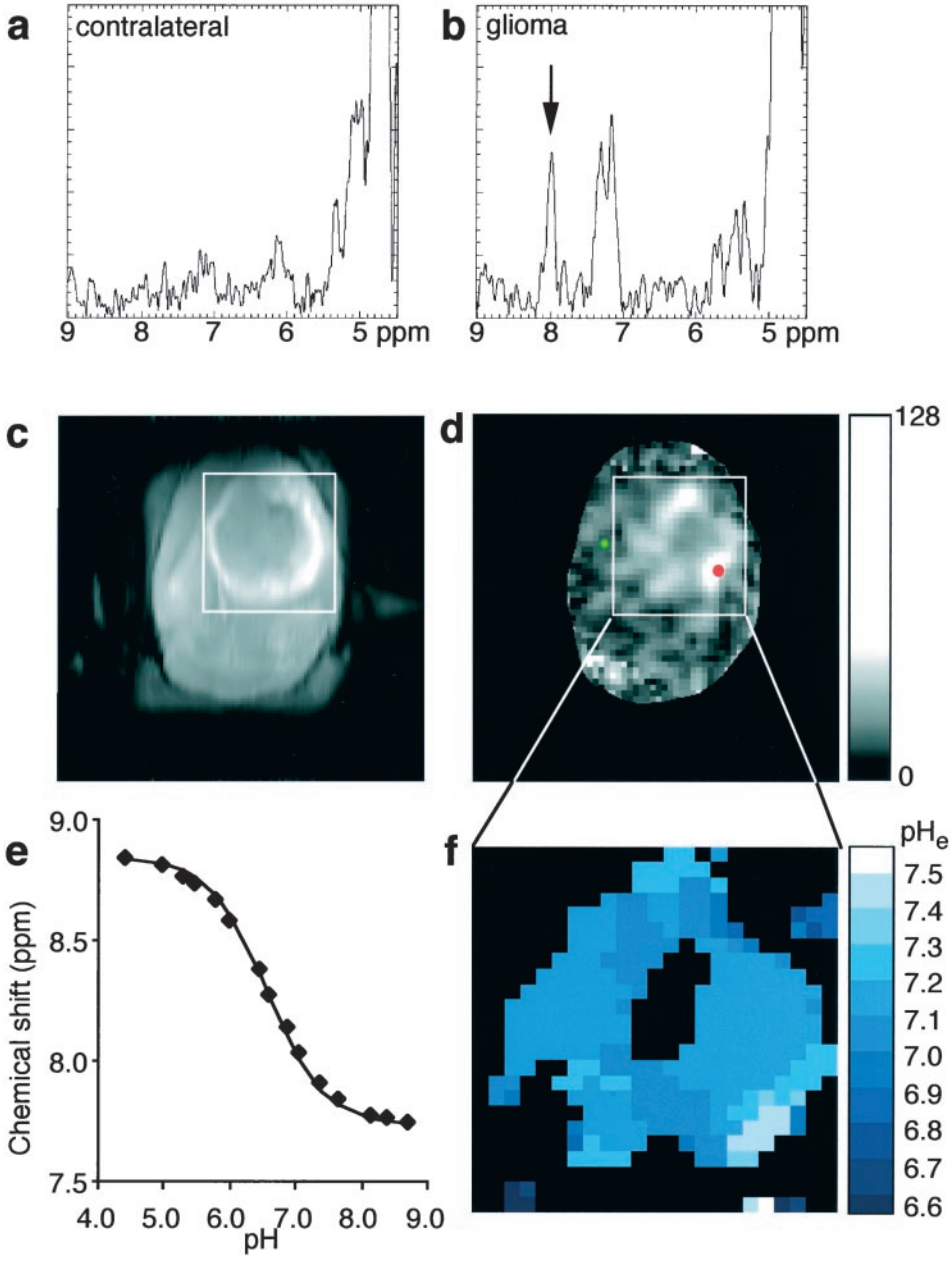

Fig. 3. *In vivo* imaging of pH_e in a glioma. After infusion of IEPA, ^1H spectra with TE = 40 ms from within the glioma (*b*) showed IEPA peaks corresponding to the pH-sensitive H2 resonance (*arrow*) and other peaks at 7.1 and 7.3 ppm; localization of the spectrum corresponds to the *red point* in *d*. IEPA peaks were not detected in the contralateral hemisphere (*a*); localization of the spectrum corresponds to the green point in (*d*). Each spectrum is presented in the magnitude mode and results from the difference between the spectrum obtained after infusion of IEPA and that obtained before. After a bolus injection of the contrast agent Gd-DOTA, an image was obtained in a horizontal section of a rat brain showing extravasation in the glioma in the right hemisphere (*c*). *d*, map of the intensity of the IEPA signals obtained in the same rat as (*c*) and at the same scale. Field homogeneity was optimized within approximately the area of the rectangle; outside this area, the signal was probably contaminated by artifacts. In *c* and *d* the selected slice was 2.5 mm thick. *e*, *in vitro* titration curve of the chemical shift of the IEPA H2 peak. *f*, map of pH_e.

contaminated the lactate peak *in vivo*. However, the IEPA methyl group peak is closer to the methylene group peak of the lipids (at 1.26 ppm). In the absence of certainty that the lipid peak was free of contamination by the IEPA peak, we have not considered the lipid distribution in this paper.

Fig. 6 illustrates for a sample glioma the seven kinds of maps that were made. As known for necrotic gliomas (35), the contrast agent Gd-DOTA, or, more strictly, the water proton hypersignal it produces on T_1-weighted images, is predominantly confined to the outer parts (Figs. 3*c* and 6, *a* and *b*). The distribution of IEPA (Fig. 6*c*) has some similarity to that of Gd-DOTA. Comparison of the Gd-DOTA distribution (Fig. 6, *a* and *b*) and the histology with maps of endogenous compounds detected by ^1H SI with a TE of 136 ms show that NAA was at a low concentration in gliomas (Fig. 6*d*). tCho or tCr tended to be present in the periphery (Fig. 6, *e* and *f*). Lactate was strongly present in outer parts of the gliomas (Fig. 6*g*); its distribution in the necrotic core could not be determined because of overlap of the (negative) lactate peak and the (positive) lipid peak. Note that Fig. 6*g* has not been corrected for this interference.

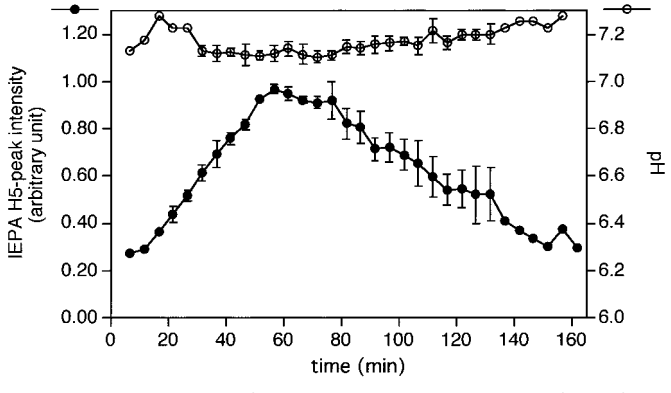

Fig. 4. Change in IEPA signal from a large voxel in the glioma during infusion of IEPA and washout. IEPA concentrations in three rats were normalized to the maximum value and averaged (*left scale*). pH_e in the glioma (*right scale, top line*) remained approximately constant. Absence of error bar indicates that a measurement was made on only one rat.

Downloaded from http://aacrjournals.org/cancerres/article-pdf/61/17/6524/2486551/ch1701006524.pdf by guest on 13 August 2024

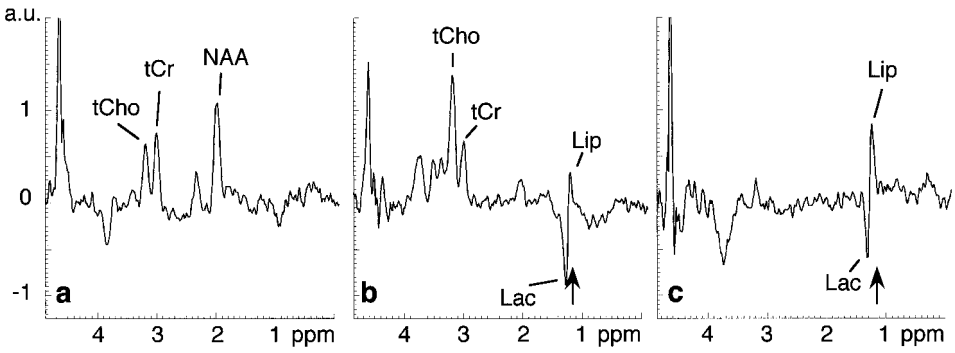

Fig. 5. Spectra (TE, 136 ms) showing peaks corresponding to metabolites. *Arrow* indicates the expected chemical shift of the protons of the IEPA methyl group. Localization of the spectra is shown on Fig. 6.

Voxel-by-Voxel Comparison of Distributions. Because the resonance peaks of the ^1H spectra were normalized with respect to the water peak, the results for the four gliomas were pooled. The various signals measured in the rectangular areas including the gliomas (as in Fig. 6*a*) were then compared, voxel-by-voxel, for the various compounds and for pH_e. Sample scatter diagrams are shown in Fig. 7. Fig. 7*a* shows that tCho and tCr, both indicative of metabolizing tissue, had, as expected, somewhat similar distributions. Lactate posed a problem because of the overlap with the lipid peak. Simulations of the two peaks showed that in voxels with no distinct lipid peak, the maximum error in the area of the lactate peak was <10%, and, for quantitative comparisons, we took into account only these voxels with no detectable lipid. In those voxels where lactate could be measured (*i.e.*, where lipids were not detected), it correlated with Gd-DOTA, a marker of extravasation through a ruptured blood-brain barrier (Fig. 7*b*).

The correlations were quantified by calculating the Pearson correlation coefficients (Eq. 2), which are given in Table 1. The coefficients for NAA are not given, because coexistence of NAA and a tumor marker occurred in only a small number of voxels at the periphery of the gliomas, which probably included both tumoral and normal tissue. Correlations for lactate were calculated only for voxels where no lipid signal was apparent. The correlations in Table 1 will be considered in the "Discussion."

DISCUSSION

Validity of the Use of IEPA to Measure pH_e. Ojugo *et al.* (6) have raised the question of the extent to which signals from an extracellular probe molecule, such as IEPA, designed to measure pH in the interstitium, are contaminated by signals from the probe in the blood, which lead to an erroneously alkaline estimate of pH_e. We suggest that the error, if any, is very small. van der Sanden *et al.* (36) have found that in 9L gliomas the blood plasma volume fraction in well-perfused parts is 0.75–1.2%, and the volume fraction of the interstitium is typically 25%, so the ratio, plasma volume:interstitium, is ~0.05. During most of the time of the IEPA imaging, IEPA was being cleared from the glioma (Figs. 1 and 4) so the concentration of IEPA in the plasma must have been less than that in the nearby interstitium. Hence, although the blood volume fraction in C6 gliomas may be higher than in 9L gliomas, the quantity of plasma IEPA in a voxel was almost certainly <10% of the quantity of interstitial IEPA. In the hypothetical case of no exchange of IEPA molecules between the blood compartment and the interstitial compartment within a voxel, one would observe, in the absence of noise, two H2 peaks with two distinct chemical shifts corresponding to the two pHs, ~7.4 in the plasma and <7.1 in the interstitium. However, with the signal:noise ratios of our spectra, the small peak corresponding to the plasma compartment would have been excluded from the analysis, and, indeed, no peak corresponding to pH ~7.4 was detected. The other extreme case, of exchange between the plasma and interstitial compartments at a rate that is high compared with the frequency difference corresponding to the two pH values is improbable but readily analyzed. In this case, there would be a single peak at a frequency corresponding to the weighted mean of the frequencies of the two component peaks (37). With our worst case assumption that the

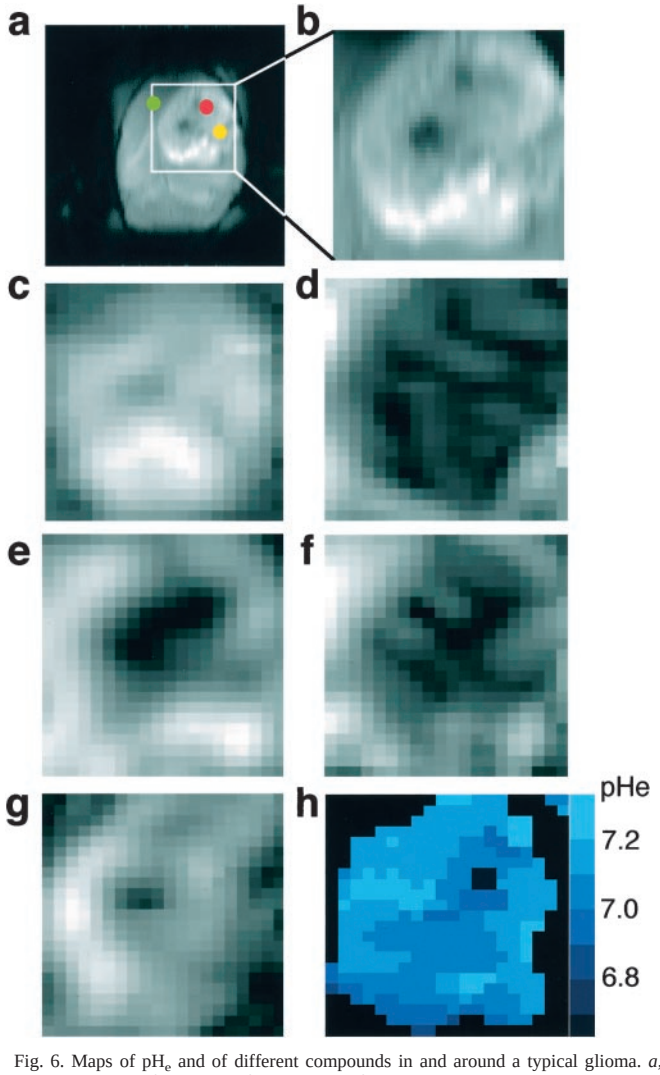

Fig. 6. Maps of pH_e and of different compounds in and around a typical glioma. *a*, T_1-weighted image of the brain after injection of Gd-DOTA showing extravasation in a glioma. *Colored points* correspond to the localization of the spectra of Fig. 5, the *green point* for the contralateral tissue, the *red point* for the necrotic part, the *yellow point* for the tumor spectrum. *b*, zoom of *a* for the rectangular area including the glioma. Maps of IEPA intensity from the H5 peak area (*c*), NAA (*d*), tCho (*e*), tCr (*f*), and lactate (*g*). *h*, map of pH_e.

Downloaded from http://aacrjournals.org/cancerres/article-pdf/61/17/6524/2486551/ch1701006524.pdf by guest on 13 August 2024

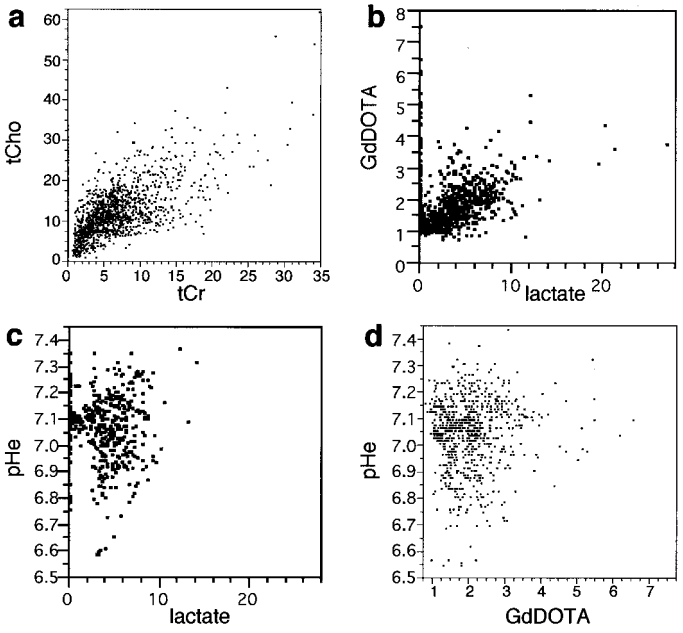

Fig. 7. Scatter diagrams of voxel-by-voxel comparisons of measured quantities within tumors and in neighboring tissue. *a* and *b*, the scales, which have arbitrary numbers, indicate the relative intensity of the signal in each voxel normalized with respect to the water peak in that voxel. tCho correlates strongly with tCr (*a*). Lactate correlates positively with the hypersignal revealed by Gd-DOTA (*b*). *c* and *d*, the ordinate gives the value of pH_e in each voxel: the correlations between pH_e and lactate concentration (*c*) is not significant and between pH_e and Gd-DOTA concentration (*d*) is slightly positive.

quantity of IEPA in the plasma is as great as 10% of the quantity in the interstitium, then the single peak would be at the interstitium frequency shifted 0.1 of the way toward the plasma frequency. Because the calibration curve (Fig. 3*e*) is nearly linear over the pH range 7.1–7.4, this shift corresponds to 0.03 pH units. This is a very conservative upper limit for the possible error introduced by the IEPA in plasma.

Another possible source of systematic error is the possible modification of pH_e by the IEPA itself. pH_e is determined by the balance between the net production (and subsequent extrusion) of proton equivalents by the cells and the clearance of the extracellular proton equivalents to the blood by diffusion through the extracellular clefts to the capillaries. pH buffer can contribute to the latter process by facilitating diffusion; flux of proton equivalents occurs not only by the diffusion of H^+ ions, which are present at a very low concentration of $\sim$0.1 μM, but also by diffusion of the buffer molecules, which may typically be present at concentrations 10^4–10^5 times greater (38). Hence, if the concentration of diffusible buffer molecules in the extracellular space was increased (by addition of IEPA), acid equivalents would be transferred more rapidly to the capillaries and the pH in the interstitium would be increased to a value closer to that of the blood (39). *A priori*, this appears to be a problem. From the measurements of [IEPA] in the glioma (Fig. 4) we estimate the maximum concentration of IEPA in the interstitium during the imaging to have been $\sim$16 mM. The major mobile pH buffer is HCO_3^-/CO_2, and the concentration of HCO_3^- in equilibrium with a P_{CO2} of 35 mm Hg at pH 7.1 is $\sim$10.5 mM. Phosphates will contribute an additional 4 mM. Although the diffusion coefficient of IEPA is smaller than those of these endogenous anions (M_r $\sim$211 *versus* 61 and 100), and it is not at its optimum pH for buffering (pK_a 6.5), IEPA may considerably increase the concentration of diffusible buffers so that pH_e is shifted in the alkaline direction. This predicted artifact might be reduced if there exist additional processes undescribed in brain interstitium, such as the contribution to facilitated diffusion by rotating proteins described *in vitro* by Gros *et al.* (40). These arguments predict that the greater the concentration of IEPA, the greater the value of pH_e. However, the experimental result of Fig. 4 shows a change in the opposite direction: as the concentration of IEPA in the glioma rose during infusion and then fell, not only did pH_e change very little, but pH_e was minimal, not maximal, when the IEPA concentration was maximal (at the end of the 60 min infusion). Another observation of the same type is that there was a significant negative correlation between the spatial distribution of IEPA and pH_e (Table 1). In conclusion, we did not observe the predicted alkalinizing effect of IEPA; either the effect was small, or it was masked by other factors that remain to be identified.

Distributions of IEPA and Gd-DOTA. Although both IEPA and Gd-DOTA were confined to the gliomas and had their highest intensities in the peripheral regions, more IEPA than Gd-DOTA was present in the center of the glioma, and the distribution of IEPA correlated less than that of Gd-DOTA with the distributions of tCho and tCr (Table 1). These observations are readily explained by the much longer infusion time for IEPA, which would have allowed it to diffuse farther away from the vasculature and into necrotic regions.

Distributions of tCho and tCr. tCr, which is associated with storage of high energy phosphate (41) and tCho, which is associated with synthesis and breakdown of membranes and with cell proliferation (42), were strongly correlated (Table 1). As shown previously for human tumors (43), tCho was highest in the periphery of the gliomas (Fig. 6*e*), and it correlated strongly with Gd-DOTA, indicating that it was in well-perfused regions (Table 1). Although the correlation coefficients were smaller, tCr was also associated with Gd-DOTA, and both tCho and tCr had positive correlations with pH_e. These results are coherent with the idea that energy metabolism and proliferation are most active in well-perfused, less acid parts of the glioma.

Distribution of Lactate. In the voxels where the lactate signal was not contaminated by a lipid signal, lactate correlated with tCho, tCr, and Gd-DOTA (Table 1), *i.e.*, it appeared to be present particularly in well-perfused, actively metabolizing parts of the glioma, in agreement with previous work (10, 44). Production of lactate under aerobic conditions is well-known for tumoral tissue (20) and has been reported recently for several kinds of normal tissue, including muscle (45), nerve (46), and brain (19). In C6 gliomas it is known that lactate is rapidly and heavily labeled from ^{14}C glucose in blood (21), and in C6 cells in culture lactate produced within the cells tends not to enter the TCA cycle (47). Hence, it is indeed to be expected that lactate is produced in the well-perfused parts of the glioma even if they are adequately oxygenated. In the center of the glioma, where we were unable to measure the relative concentration of lactate, we would expect it to be at least as high as the interstitial concentration in the outer parts, even if no lactate were produced there because it would

Table 1 *Voxel-by-voxel correlations*

Scatter diagrams, such as those in Fig. 6, were analyzed by calculating the Pearson correlation coefficients (Eq. 2). For metabolites except for lactate, all 1621 voxels from the rectangular areas selected for the four rats were included. Lactate was calculated in the 840 voxels where no lipid signal was detected. pH_e was calculated in the 776 voxels where the IEPA H2 peak was measurable.

	Lactate	tCho	tCr	Gd-DOTA	IEPA
pH_e	NS[a]	0.199[b]	0.128[c]	0.071[d]	−0.176[b]
Lactate		0.284[b]	0.117[c]	0.296[b]	NS[a]
tCho			0.629[b]	0.591[b]	0.052[d]
tCr				0.295[b]	NS[a]
Gd-DOTA					0.230[b]

[a] NS, $P > 0.05$ are not significant.
[b] $P < 0.0001$.
[c] $P < 0.001$.
[d] $P < 0.05$.

Downloaded from http://aacrjournals.org/cancerres/article-pdf/61/17/6524/2486551/ch1701006524.pdf by guest on 13 August 2024

tend to be in diffusional equilibrium. However, in the solid parts of the tumor, most of the lactate is expected to be intracellular. This is not only because the intracellular volume fraction is greater than the extracellular volume fraction, but the intracellular concentration of lactate will be higher than the extracellular concentration. Lactate can readily cross the plasma membrane of most cells (including Ehlrich tumor cells; Ref. 48) by passive cotransport with protons, so that the concentrations of the neutral protonated form, Hlactate, inside and outside the cell tend to equilibrate (22). Within each compartment (intracellular and extracellular) the ratio of [Hlactate]:[lactate$^-$] is determined by the pH according to the Henderson-Hasselbalch equation. It follows that because $[Hlactate]_i \approx [Hlactate]_e$, [total intracellular lactate]/[total extracellular lactate] $\sim [H^+]_e/[H^+]_i$ (see Ref. 49). pH_i in C6 gliomas is $\geq$7.2 (50), so $[H^+]_e/[H^+]_i > 1$, so [total lactate]$_i >$ [total lactate]$_e$. Hence in the viable parts of the glioma, total lactate will be mainly ($\approx$80%) intracellular, partly because intracellular space constitutes most of the volume, and partly because [total lactate] is somewhat higher within this space.

Distribution of pH_e in the Gliomas. Although, as explained above, we cannot completely exclude the possibility that the contribution of IEPA to facilitated diffusion of protons through the extracellular clefts increases the absolute values of pH_e, spatial variations in pH_e should nevertheless be detected. On a scale of mm, pH_e showed variations on the order of 0.1 pH units (at least within that part of the glioma into which IEPA diffused), in agreement with Ref. 10. However, the variations do not follow a regular geometry, and our data do not reveal the presence of an average gradient of pH_e from the core toward the periphery in the C6 glioma model.

Although we found spatial variations of pH_e of $<$0.1 pH unit mm^{-1}, Helmlinger *et al.* (15) reported that measurements made on s.c. tumors with a fluorescent pH probe, which gave a higher spatial resolution, showed that gradients of pH_e close to blood vessels can be very steep: $>$0.4 pH units/100 μm. Hence, the value we obtained for each voxel is the average of what may be a range of values of pH_e.

Comparison of the Distributions of Lactate and pH_e. Although the formation of lactate from pyruvate consumes rather than produces protons, the overall pathway of glycolysis from glucose to lactate results in the net production of 2 ATP, which produce 1 H^+ per ATP when dephosphorylated to ADP. One glucose molecule also produces two lactate ions, which will be cotransported out of the cell with two H^+, so although pH_e will decrease there is no tendency for pH_i to change. In contrast to glycolysis, full oxidation of glucose consumes protons that just balance the production of H^+ by hydrolysis of ATP; however, there is production of CO_2 (which reacts with H_2O to give H^+) but at a rate of only 1 CO_2/6 ATP (51). Because a cell requires a certain amount of ATP to function, it is clear that if glycolysis replaces oxidative phosphorylation as a major source of ATP, then more H^+ equivalents will be exported to the extracellular space. In general, this is true: pH_e is indeed more acid in lactate-producing tumors than in normal tissue. Therefore, it is striking that within the gliomas (at least in the parts with no detectable lipid signal) our results show no significant negative correlation of lactate signal with pH_e (Table 1). A possible explanation is that most lactate is produced in well-perfused regions with viable cells and that in these regions H^+ can diffuse away to the blood stream more readily than lactate can.

We have demonstrated that a new probe molecule, IEPA, can be used for imaging pH_e in a rat brain glioma model *in vivo*. This new technique made it possible to perform ^{1}H SI in the same experiments. By comparing quantitatively the distributions of different metabolites, Gd-DOTA and pH_e, no evidence was observed that pH_e was significantly lower where lactate concentration was higher, and we reach the conclusion that lactate production is greatest in well-perfused parts of gliomas.

ACKNOWLEDGMENTS

IEPA was synthesized by ROVI Pharmaceutical Laboratories, Madrid, Spain, and used with their permission. We thank Michel Décorps for critical discussion. The surface coil was constructed by Olivier Montigon.

REFERENCES

1. Wike-Hooley, J. L., Haveman, J., and Reinhold, H. S. The relevance of tumor pH to the treatment of malignant disease. Radiother. Oncol., *2:* 343–366, 1984.
2. Kallinowski, F., and Vaupel, P. pH distributions in spontaneous and isotransplanted rat tumours. Br. J. Cancer, *58:* 314–321, 1988.
3. Stubbs, M., McSheehy, P. M., and Griffiths, J. R. Causes and consequences of acidic pH in tumors: a magnetic resonance study. Adv. Enzyme Regul., *39:* 13–30, 1999.
4. Gerweck, L. E., and Seetharaman, K. Cellular pH gradient in tumor *versus* normal tissue: potential exploitation for the treatment of cancer. Cancer Res., *56:* 1194–1198, 1996.
5. Gerweck, L. E., Kozin, S. V., and Stocks, S. J. The pH partition theory predicts the accumulation and toxicity of doxorubicin in normal and low-pH-adapted cells. Br. J. Cancer, *79:* 838–842, 1999.
6. Ojugo, A. S. E., McSheehy, P. M. J., McIntyre, D. J. O., McCoy, C. L., Stubbs, M., Leach, M. O., Judson, J. R., and Griffiths, J. R. Measurement of the extracellular pH of solid tumors in mice by magnetic resonance spectroscopy: a comparison of exogenous ^{19}F and ^{31}P probes. NMR Biomed., *12:* 495–504, 1999.
7. Raghunand, N., He, X., van Sluis, R., Mahoney, B., Baggett, B., Taylor, C. W., Paine-Murrieta, G., Roe, D., Bhujwalla, Z. M., and Gillies, R. J. Enhancement of chemotherapy by manipulation of tumour pH. Br. J. Cancer, *80:* 1005–1011, 1999.
8. Engin, K., Leepers, D. B., Thistlethwaite, A. J., Tupchong, L., and McFarlane, J. D. Tumor extracellular pH as a prognostic factor in thermoradiotherapy. Int. J. Radiat. Oncol. Biol. Phys., *29:* 125–132, 1994.
9. Pampus, F. Die Wasserstoffionenkonzentration des Hirngewebes bei raumfordernden intracraniellen Prozessen. Acta Neurochir., *11:* 305–318, 1963.
10. Jahde, E., Rajewsky, M. F., and Baumgartl, H. pH distributions in transplanted neural tumors and normal tissues of BDIX rats as measured with pH microelectrodes. Cancer Res., *42:* 1498–1504, 1982.
11. Jayasundar, R., Honess, D., Hall, L. D., and Bleehen, N. M. Simultaneous evaluation of the effects of RF hyperthermia on the intra- and extracellular tumor pH. Magn. Reson. Med., *43:* 1–8, 2000.
12. Gillies, R. J., Liu, Z., and Bhujwalla, Z. M. 31P-MRS measurements of extracellular pH of tumors using 3-aminopropylphosphonate. Am. J. Physiol, *267:* C195–C203, 1994.
13. McCoy, C. L., Parkins, C. S., Chaplin, D. J., Griffiths, J. R., Rodrigues, L. M., and Stubbs, M. The effect of blood flow modification on intra- and extracellular pH measured by ^{31}P magnetic resonance spectroscopy in murine tumours. Br. J. Cancer, *72:* 905–911, 1995.
14. Aoki, Y., Akagi, K., Tanaka, Y., Kawai, J., and Takahashi, M. Measurement of intratumor pH by pH indicator used in 19F-magnetic resonance spectroscopy. Measurement of extracellular pH decrease caused by hyperthermia combined with hydralazine. Investig. Radiol., *31:* 680–689, 1996.
15. Helmlinger, G., Yuan, F., Dellian, M., and Jain, R. K. Interstitial pH and PO_2 gradients in solid tumors *in vivo*: high resolution measurements reveal a lack of correlation. Nat. Med., *3:* 177–182, 1997.
16. Gil, S., Zaderenzo, P., Cruz, F., Cerdan, S., and Ballesteros, P. Imidazol-1-ylalkanoate acids as extrinsic ^{1}H NMR probes for the determination of intracellular pH, extracellular pH and cell volume. Bioorg. Med. Chem., *2:* 305–314, 1994.
17. van Sluis, R., Bhujwalla, Z. M., Raghunand, N., Ballesteros, P., Alvarez, J., Cerdan, S., Galons, J. P., and Gillies, R. J. *In vivo* imaging of extracellular pH using 1H MRSI. Magn. Reson. Med., *41:* 743–750, 1999.
18. García-Martín, M. L., Hérigault, G., Rémy, C., Farion, R., Ballesteros, P., Coles, J. A., Cerdán, S., and Ziegler, A. ^{1}H magnetic resonance spectroscopic imaging of extracellular pH in an intracerebral glioma. Proc. Intl. Soc. Mag. Reson. Med., *8:* 1029, 2000.
19. Pfeuffer, J., Tkác, I., Choi, I-Y., Merkle, H., Ugurbil, K., Garwood, M., and Gruetter, R. Localized *in vivo* ^{1}H NMR detection of neurotransmitter labeling in rat brain during infusion of [1-^{13}C] D-glucose. Magn. Reson. Med., *41:* 1077–1083, 1999.
20. Warburg, O., and Minani, S. Versuche an überlebendem Carcinomgewebe. Klin. Wochenschr., *2:* 776–777, 1923.
21. Terpstra, M., Gruetter, R., High, W. B., Mescher, M., DelaBarre, L., Merkle, H., and Garwood, M. Lactate turnover in rat glioma measured by *in vivo* nuclear magnetic resonance spectroscopy. Cancer Res., *58:* 5083–5088, 1998.
22. Halestrap, A. P., and Price, N. T. The proton-linked monocarboxylate transporter (MCT) family: structure, function and regulation. Biochem. J., *343 Pt 2:* 281–299, 1999.
23. Yamagata, M., Hasuda, K., Stamato, T., and Tannock, I. F. The contribution of lactic acid to acidification of tumours: studies of variant cells lacking lactate dehydrogenase. Br. J. Cancer, *77:* 1726–1731, 1998.
24. Newell, K., Franchi, A., Pouyssegur, J., and Tannock, I. Studies with glycolysis-deficient cells suggest that production of lactic acid is not the only cause of tumor acidity. Proc. Natl. Acad. Sci. USA, *90:* 1127–1131, 1993.
25. von Kienlin, M., Décorps, M., Albrand, J-P., Foray, M-F., and Blondet, P. Hard-pulse sequences for solvent suppression which only need a zero-order phase correction. J. Magn. Reson., *76:* 169–173, 1988.
26. Benda, P., Lightbody, J., Sato, G., Levine, L., and Sweet, W. Differentiated rat glial cell strain in tissue culture. Science (Wash. DC), *161:* 370–371, 1968.
27. Kobayashi, N., Allen, N., Clendenon, N. R., and Ko, L. W. An improved rat brain-tumor model. J. Neurosurg., *53:* 808–815, 1980.

Downloaded from http://aacrjournals.org/cancerres/article-pdf/61/17/6524/2486551/ch1701006524.pdf by guest on 13 August 2024

28. Le Duc, G., Peoc'h, M., Rémy, C., Charpy, O., Muller, R. N., Le Bas, J. F., and Décorps, M. Use of T(2)-weighted susceptibility contrast MRI for mapping the blood volume in the glioma-bearing rat brain. Magn. Reson. Med., *42:* 754–761, 1999.
29. Bottomley, P. A. Spatial localization in NMR spectroscopy *in vivo*. Ann. N. Y. Acad. Sci., *508:* 333–348, 1987.
30. Haase, A., Frahm, J., Hänicke, W., and Matthaei, D. ^{1}H NMR chemical shift selective (CHESS) imaging. Phys. Med. Biol., *30:* 341–344, 1985.
31. Plateau, P., Dumas, C., and Guéron, M. Solvent-peak-suppressed, NMR correction of baseline distortions and use of a strong-pulse excitation. J. Magn. Reson., *54:* 46–53, 1983.
32. Hore, P. Solvent suppression in fourier transform nuclear magnetic resonance. J. Magn. Reson., *55:* 283–300, 1983.
33. Hodgkinson, P., and Hore, P. J. Optimizing spatially localized NMR. J. Magn. Reson. B, *106:* 261–269, 1995.
34. Govindaraju, V., Young, K., and Maudsley, A. A. Proton NMR chemical shifts and coupling constants for brain metabolites. NMR Biomed., *13:* 129–153, 2000.
35. Schorner, W., Laniado, M., Niendorf, H. P., Schubert, C., and Felix, R. Time-dependent changes in image contrast in brain tumors after gadolinium-DTPA. Am. J. Neuroradiol., *7:* 1013–1020, 1986.
36. van der Sanden, B. P., Rozijn, T. H., Rijken, P. F., Peters, H. P., Heerschap, A., van der Kogel, A. J., and Bovee, W. M. Noninvasive assessment of the functional neovasculature in 9L-glioma growing in rat brain by dynamic ^{1}H magnetic resonance imaging of gadolinium uptake. J. Cereb. Blood Flow Metab., *20:* 861–870, 2000.
37. Gadian, D. G. (ed.). NMR and its Applications to Living Systems, Ed. 2, Oxford: Oxford University Press, 1995.
38. Engasser, J. M., and Horvath, C. Buffer-facilitated proton transport pH profile of bound enzymes. Biochim. Biophys. Acta, *358:* 178–192, 1974.
39. Griffiths, J. R., McIntyre, D. J. O., Howe, F. A., and Stubbs, M. Why are cancers acidic? A carrier-mediated diffusion model for H^+ transport in the interstitial fluid. *In:* R. J. Gillies (ed.), Causes and Consequences of Acidic pH in Tumors, Vol. in press,. New York: Wiley, 2001.
40. Gros, G., Lavalette, D., Moll, W., Gros, H., Amand, B., and Pochon, F. Evidence for rotational contribution to protein-facilitated proton transport. Proc. Natl. Acad. Sci. USA, *81:* 1710–1714, 1984.
41. Hilberman, M., Subramanian, V. H., Haselgrove, J., Cone, J. B., Egan, J. W., Gyulai, L., and Chance, B. *In vivo* time-resolved brain phosphorus nuclear magnetic resonance. J. Cereb. Blood Flow Metab., *4:* 334–342, 1984.
42. Tamiya, T., Kinoshita, K., Ono, Y., Matsumoto, K., Furuta, T., and Ohmoto, T. Proton magnetic resonance spectroscopy reflects cellular proliferative activity in astrocytomas. Neuroradiology, *42:* 333–338, 2000.
43. Segebarth, C. M., Baleriaux, D. F., Luyten, P. R., and den Hollander, J. A. Detection of metabolic heterogeneity of human intracranial tumors *in vivo* by ^{1}H NMR spectroscopic imaging. Magn. Reson. Med., *13:* 62–76, 1990.
44. Terpstra, M., High, W. B., Luo, J., de Graaf, R. A., Merkle, H., and Garwood, M. Relationships among lactate concentration, blood flow and histopathologic profiles in rat C6 glioma. NMR Biomed., *9:* 185–194, 1996.
45. Kemper, W. F., Lindstedt, S. L., Hartzler, L. K., Hicks, J. W., and Conley, K. E. Shaking up glycolysis: sustained, high lactate flux during aerobic rattling. Proc. Natl. Acad. Sci. USA, *98:* 723–728, 2001.
46. Véga, C., Poitry-Yamate, C. L., Jirounek, P., Tsacopoulos, M., and Coles, J. A. Lactate is released and taken up by isolated rabbit vagus nerve during aerobic metabolism. J. Neurochem., *71:* 330–337, 1998.
47. Bouzier, A. K., Goodwin, R., de Gannes, F. M., Valeins, H., Voisin, P., Canioni, P., and Merle, M. Compartmentation of lactate and glucose metabolism in C6 glioma cells. A 13c and ^{1}H NMR study. J. Biol. Chem., *273:* 27162–27169, 1998.
48. Carpenter, L., Poole, R. C., and Halestrap, A. P. Cloning and sequencing of the monocarboxylate transporter from mouse Ehrlich Lettre tumour cell confirms its identity as MCT1 and demonstrates that glycosylation is not required for MCT1 function. Biochim. Biophys. Acta, *1279:* 157–163, 1996.
49. Thomas, R. C. Experimental displacement of intracellular pH and the mechanism of its subsequent recovery. J. Physiol. (Lond.), *354:* 3P–22P, 1984.
50. Froissart-Rémy, C. Intérêt de la spectroscopie RMN pour l'étude *in vivo* du métabolisme cérébral dans le cas de pathologies globales et localisées. Thesis no. 90/GRE/110. pp. 514. Grenoble: Université Joseph Fourier, 1990.
51. Krebs, H. A., Woods, H. F., and Alberti, K. G. M. M. Hyperlactatemia and lactic acidosis. Essays Med. Biochem., *1:* 81–103, 1975.

Downloaded from http://aacrjournals.org/cancerres/article-pdf/61/17/6524/2486551/ch1701006524.pdf by guest on 13 August 2024